Received: 20 January 2016 | Revised: 1 July 2016 | Accepted: 15 July 2016

DOI 10.1111/cmi.12650

WILEY

RESEARCH ARTICLE

Differential time-dependent volumetric and surface area changes and delayed induction of new permeation pathways in *P. falciparum*-infected hemoglobinopathic erythrocytes

Mailin Waldecker[1] | Anil K. Dasanna[2,3] | Christine Lansche[1] | Marco Linke[2,3] | Sirikamol Srismith[1] | Marek Cyrklaff[1] | Cecilia P. Sanchez[1] | Ulrich S. Schwarz[2,3] | Michael Lanzer[1*]

[1] Department of Infectious Diseases, Parasitology, Heidelberg University, Medical School, Im Neuenheimer Feld 324, Heidelberg 69120, Baden-Württemberg, Germany

[2] BioQuant, Heidelberg University, Im Neuenheimer Feld 267, Heidelberg 69120, Baden-Württemberg, Germany

[3] Institute for Theoretical Physics, Heidelberg University, Philosophenweg 19, Heidelberg 69120, Baden-Württemberg, Germany

Correspondence
Michael Lanzer, Dept. of Infectious Diseases, Parasitology, Heidelberg University, Medical School Im Neuenheimer Feld 324, Heidelberg 69120, Baden-Württemberg, Germany.
Email: michael.lanzer@med.uni-heidelberg.de

Abstract

During intraerythrocytic development, *Plasmodium falciparum* increases the ion permeability of the erythrocyte plasma membrane to an extent that jeopardizes the osmotic stability of the host cell. A previously formulated numeric model has suggested that the parasite prevents premature rupture of the host cell by consuming hemoglobin (Hb) in excess of its own anabolic needs. Here, we have tested the colloid-osmotic model on the grounds of time-resolved experimental measurements on cell surface area and volume. We have further verified whether the colloid-osmotic model can predict time-dependent volumetric changes when parasites are grown in erythrocytes containing the hemoglobin variants S or C. A good agreement between model-predicted and empirical data on both infected erythrocyte and intracellular parasite volume was found for parasitized HbAA and HbAC erythrocytes. However, a delayed induction of the new permeation pathways needed to be taken into consideration for the latter case. For parasitized HbAS erythrocyte, volumes diverged from model predictions, and infected erythrocytes showed excessive vesiculation during the replication cycle. We conclude that the colloid-osmotic model provides a plausible and experimentally supported explanation of the volume expansion and osmotic stability of *P. falciparum*-infected erythrocytes. The contribution of vesiculation to the malaria-protective function of hemoglobin S is discussed.

1 | INTRODUCTION

Plasmodium falciparum, the etiologic agent of tropical malaria and a leading cause of childhood mortality in developing countries (World Health Organization, 2015), is an obligatory intracellular parasite. *P. falciparum* initially replicates in human hepatocytes, following transmission by the bite of an infected, blood sucking *Anopheles* mosquito, before the parasite changes its host cell specificity and infects erythrocytes. Because intraerythrocytic development of *P. falciparum* causes most of the pathology associated with malaria, substantial effort has been paid to understand the interactions between the parasite and the infected erythrocyte at the molecular level. Early on, it was recognized that the parasite ingests large amounts of hemoglobin; some studies point to a reduction in hemoglobin content between 65 and 80% (Elliott et al., 2008; Krugliak, Zhang, & Ginsburg, 2002). However, when the fate of the liberated amino acids was investigated, it was found that less than 25% of them are reused by the parasite for de novo protein synthesis (Krugliak et al., 2002). The majority is released into the extracellular environment. There has been much speculation about the reason for this seemingly wasteful spending and why the parasite invests such a considerable amount of energy in enzymatically degrading hemoglobin when it does not completely use the proteolytic products for its own anabolism (Rosenthal, 2011).

An ingenious hypothesis to explain this conundrum was formulated by Lew, Tiffert, and Ginsburg (2003) (Lew et al., 2003; Lew, Macdonald, Ginsburg, Krugliak, & Tiffert, 2004; Mauritz et al., 2009). They recognized that hemoglobin digestion coincides concurrently

with another parasite-induced alteration to the infected erythrocyte, namely, increased solute traffic across the erythrocyte plasma membrane via parasite-encoded channels (also referred to as new permeation pathways, NPPs) (Desai, 2012; Ginsburg, Kutner, Krugliak, & Cabantchik, 1985; Ginsburg & Stein, 2004). If uninfected erythrocytes were permeabilized to the same extent, they would hemolyze by the osmotic pressure generated by the influx of NaCl and osmotic water (Staines, Ellory, & Kirk, 2001). Hemolysis would occur in spite of the fact that erythrocytes have the capacity to increase their volume by 70% before they rupture (Ponder, 1948), as the infected erythrocyte changes its shape from a biconcave discoid to a sphere during the swelling process. Given that hemoglobin is a membrane impermeable anion that draws ions and accompanying water into the cell (thereby acting as a colloid), digesting it and expelling the remains might maintain the colloid-osmotic balance within the infected erythrocyte and thus prevent premature lysis.

To validate the colloid-osmotic model, Lew et al. (2003) simulated the volume expansion of both the parasitized erythrocyte and the parasite itself during the 48-hr replicative cycle, taking into account numerous physiological and kinetic parameters relevant to the control of cell volume, including pH, parasite growth rate, ion fluxes across the erythrocyte plasma membrane, intracellular and extracellular ion concentrations, and hemoglobin consumption (Lew et al., 2003; Mauritz et al., 2009). The mathematical model predicts that the volume of the infected erythrocyte remains constant at the value of the uninfected erythrocyte for the first 20 hr of parasite development. This quiescent phase is then followed by a transient shrinkage brought about by a predicted K^+-driven net fluid loss. As the parasite-encoded channels are activated in the erythrocyte plasma membrane, the electrochemical gradients of K^+ and Na^+ gradually dissipate, however, not at equal rates because K^+ is thought to have a 2.3-fold higher permeability than Na^+ does (Staines et al., 2001). As a result, KCl efflux transiently exceeds NaCl influx. The ensuing net loss of salt and accompanying water lets the cell shrink until the moment when the K^+ gradient is dissipated. From then on, the infected erythrocyte swells because of Na^+-driven fluid gain. The digestion of hemoglobin relieves some of the osmotic pressure, according to the model. Yet the infected erythrocyte continues to swell until it approaches the critical hemolytic volume at the end of the 48-hr cycle.

The numeric model also predicts the parasite volume. Given that the parasite takes up hemoglobin by endocytosis of the host cytoplasm, parasite volume growth is linked to hemoglobin incorporation and defined as the cumulative volume of endocytosed host cytoplasm at a given time in the replicative cycle (Lew et al., 2003; Mauritz et al., 2009). The homeostatic factors that affect the volume of the host cytosol being incorporated by the parasite are taken into account when simulating the parasite's volume.

As attractive as the colloid-osmotic model seems, some questions have been raised (Allen & Kirk, 2004). The model was particularly challenged on the grounds of inconsistencies in volume predictions with available experimental data, with the numeric model seemingly overestimating both parasite and infected cell volume (Allen & Kirk, 2004). Lew and colleagues addressed this concern by proposing an 18% surface area loss between the trophozoite (24–36 hr post invasion) and the schizont stage (36 to 48 hr post invasion) (Esposito et al., 2010). Because a fractional reduction in the surface area propagates to a fractional reduction in volume to the power of 1.5, assuming a sphere, the loss in host cell membrane would increase the osmotic fragility of the infected erythrocyte and, hence, reconcile the colloid-osmotic model with the experimental volume determinations (Mauritz et al., 2009).

A full evaluation of the colloid-osmotic model and its ramifications is hampered by a lack of robust experimental data on the volumes of the parasitized erythrocyte and the intracellular parasite. The few available determinations refer to single measurements, and no attempt has been made to systematically investigate the temporal changes in cell volume throughout the intraerythrocytic life cycle (Elliott et al., 2008; Elliott, Saliba, & Kirk, 2001; Saliba, Horner, & Kirk, 1998; Zanner, Galey, Scaletti, Brahm, & Vander Jagt, 1990).

If excessive hemoglobin consumption prevents infected erythrocytes from premature lysis, as postulated by the colloid-osmotic model, then this claim should apply to any red blood cell variant in which the parasite propagates—not just HbAA erythrocytes for which the model was originally developed. Malaria endemic areas are characterized by a high prevalence of hemoglobinopathies, including the sickle cell hemoglobin S (HbS) and hemoglobin C (HbC) (Kwiatkowski, 2005). Carriers of these traits have a selective advantage in *P. falciparum* infections and are protected from severe malaria-related disease and death (Cholera et al., 2008; Fairhurst et al., 2005; Modiano et al., 2001; Taylor, Parobek, & Fairhurst, 2012), which explains why these hemoglobinopathies have emerged and spread under the evolutionary pressure of malaria. HbS and HbC are each single amino acid polymorphisms in the ß-globin chain of hemoglobin (Hb), which consists of two α- and two ß-globin chains. In HbS and HbC, the glutamic acid at position 6 in the ß-globin chain is substituted by valine and lysine, respectively.

Hemoglobin S affects many morphological and physiological functions of the red blood cell (Hebbel, 1991). This includes increased ion permeability, augmented osmotic fragility, and defects in membrane skeletal organization (Hebbel, 1991; Lew & Bookchin, 2005). At low oxygen tension, HbS tends to polymerize when present in homozygous form or as heterozygous HbSC, causing sickling of the erythrocyte (Hebbel, 1991; Nagel, Fabry, & Steinberg, 2003). Patients carrying the HbSS or HbSC alleles frequently develop sickle cell disease (Hannemann et al., 2011; Turgeon, 2011). The consequences of HbC on red blood cell physiology are less severe and include reduced cell deformability and dehydration (Turgeon, 2011). Heterozygous HbAC is a benign condition, with no clinical consequences. The homozygous form, however, can cause HbC disease, which is associated with a mild degree of hemolytic anemia, splenomegaly, and the formation of microspherocytes and HbC crystals (Dalia & Zhang, 2013; Fairhurst & Casella, 2004; Turgeon, 2011). Given that *P. falciparum* replicates within heterozygous HbAS and HbAC erythrocytes with normal rates under optimal in vitro culture conditions (Table 1) (Kilian et al., 2013; Kilian et al., 2015), one wonders whether the colloid-osmotic model can also account for the osmotic stability of these cells during a *P. falciparum* infection.

Here, we have examined the colloid-osmotic model, by challenging the simulated volumetric predictions with experimental determinations. A high agreement between simulated and empirical data was found for parasitized HbAA erythrocytes. The numeric model could also correctly predict the expansion of erythrocyte and parasite volume during intraerythrocytic development in HbAC erythrocytes, provided that the delayed activation of the NPPs, as was observed in

TABLE 1 Replication rates and hemozoin production of the *Plasmodium falciparum* strain FCR3 grown in different erythrocyte variants

Hb variant	Replication rate per cycle	Normalized amount of hemozoin (%)
HbAA	11 ± 1 (10)	100 ± 5 (10)
HbAS	12 ± 1 (10)	98 ± 22 (10)
HbAC	11 ± 1 (10)	110 ± 8 (10)

The amount of hemozoin was determined in late trophozoites and normalized to the amount determined in infected HbAA erythrocytes. The means ± SD of (*n*) determinations is shown. There was no statistically significant difference between the groups with regard to the replication rate (p = .719) or the amount of hemozoin produced (p = .785), according to a one-way analysis of variance test.

Hb, hemoglobin.

parasitized HbAC erythrocytes, was taken into consideration. The numeric model, however, was less successful in simulating volume expansions in parasitized HbAS erythrocytes.

2 | RESULTS

2.1 | Infected cell and parasite volume expansion in parasitized HbAA erythrocytes

To obtain surface and volumetric data on infected and uninfected erythrocytes, we developed the following work flow: Cells were stained with the fluorescent membrane dye BODIPY TR Ceramid and imaged using a confocal fluorescence microscope. Approximately 60 consecutive serial sections were recorded for each cell (Figure 1a), from which surface rendered views were generated (Figure 1b). Cell surface area and volume were subsequently calculated from the surface rendered views using triangulation (Figure 1c).

To validate our method, we investigated uninfected erythrocytes from two HbAA, HbAS, and HbAC donors each and then compared the results with those obtained using an automated blood cell counter certified and used for diagnostic purposes (Table 2). Our volumetric

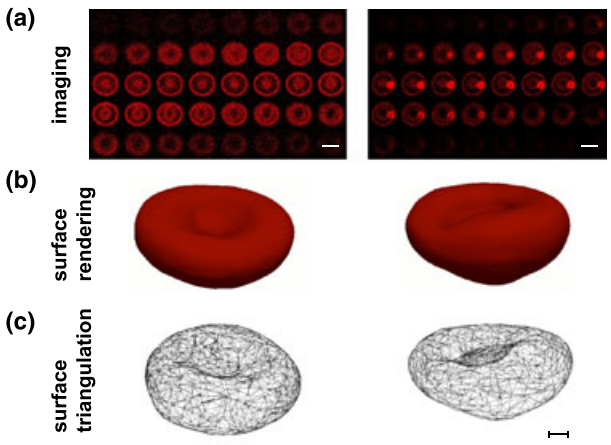

FIGURE 1 From confocal images to mesoscopic models. (a) Consecutive confocal images of a BODIPY TR Ceramid stained uninfected (left panel) and infected HbAA erythrocyte (right panel; ring stage parasite) are shown. White scale bar, 5 μM. (b) Corresponding surface rendered views. (c) The mesoscopic representations of the cell surface by a triangulated mesh. Black scale bar, 1 μm

determinations were in good agreement with those made by the blood cell analyzer, according to the Bland-Altman methods comparison test (Bland & Altman, 1986) (supplementary Figure S1). Moreover, the sample variance observed using our imaging technique was in the range of what would be expected based on natural red blood cell heterogeneity (Table 2 and supplementary Figure S2) (Turgeon, 2011). The automated blood cell counter did not provide data on the cell surface area, precluding a comparative analysis of this parameter. Since the imaging technique provided more information regarding cell geometry and cell shape compared with the blood cell analyzer, we decided to use this method throughout the study.

Having established that our approach produced reliable and robust surface and volumetric data for red blood cells, we next analyzed HbAA erythrocytes infected with the *P. falciparum* strain FCR3 at different stages of parasite development. To this end, samples were taken from highly synchronized cultures in 4-hr intervals throughout the intraerythrocytic life cycle. For each time point an average of 10 single cells were processed and each time course was reproduced three times using blood from different donors. Representative examples of reconstructed surfaces are shown in Figure 2a and 2b. The results were subsequently normalized to the corresponding uninfected erythrocytes. As shown in Figure 3a, the relative surface area of the infected erythrocyte remained constant throughout the 48-hr life cycle of the parasite. This conclusion was verified by fitting a linear regression to the data points, which gave a slope not significantly different from zero. Reanalyzing the data by grouping them into ring (0 to 20 hr post invasion), trophozoite (24 to 36 hr post invasion), and schizont stages (40 to 48 hr post invasion) confirmed that the host cell surface area did not statistically differ between the different stages and between infected and uninfected erythrocytes (Figure 3b).

Previous studies have used the term reduced volume to describe, in numerical terms, shape transformations of red blood cells (Lim, Wortis, & Mukhopadhyay, 2002; Lim, Wortis, & Mukhopadhyay, 2008). The reduced volume is defined here as the ratio of the actual red blood cell volume to the volume of a sphere having the same surface area. Applying the concept of reduced volume to parasitized erythrocytes revealed that this parameter significantly increased from .63 to .99 in a sigmoidal fashion with time, with the inflection point at approximately 34 ± 3 hr post invasion (p < .01; Figure 3c). The significant gradual increase in reduced volume was confirmed by grouping the data according to the three major parasite stages (Figure 3d). Given that the reduced volume of an ideal sphere is 1.0, this finding indicates that the shape of the parasitized erythrocyte changed from a biconcave discoid to a spherical morphology as the parasite matured within its host cell, consistent with the surface rendered views shown in Figure 2a and previous reports (Esposito et al., 2010; Nash, O'Brien, Gordon-Smith, & Dormandy, 1989).

The change in reduced volume coincided with a significant relative cell volume expansion during the time course of parasite development (p < .01; Figure 4a and b). While the relative volume of the infected erythrocyte remained close to that of the uninfected erythrocyte for the first 28 hr post invasion, it dramatically increased, in a hyperbolic fashion, in the following hours until the volume reached 1.6-fold of its initial value at the end of the 48-hr cycle. Taking into account the variance in the data of approximately 10%, the volume of the infected erythrocytes approached the critical hemolytic volume at the right

TABLE 2 Erythrocyte parameters form different blood donors and using different measurement methods

Hb variant	MCV[a] µm³	MCHC[b] g/dl	RDW[c] %	Volume µm³	Surface area µm²	Reduced volume
HbAA donor 1	87 ± 11 (1000)	35	13.0	83 ± 10 (19)	136 ± 11	.56 ± .05
HbAA donor 2	91 ± 11 (1000)	35	12.2	96 ± 18 (10)	136 ± 12	.64 ± .08
HbAS donor 3	82 ± 12 (1000)	35	13.1	90 ± 15 (17)	131 ± 11	.64 ± .08
HbAS donor 4	82 ± 11 (1000)	34	14.8	84 ± 10 (30)	135 ± 10	.57 ± .04
HbAC donor 5	81 ± 13 (1000)	33	16.2	76 ± 9 (15)	126 ± 9	.53 ± .13
HbAC donor 6	78 ± 12 (1000)	33	15.5	87 ± 9 (14)	141 ± 11	.57 ± .03

[a]Normal value range: 80–100 µm³ (Turgeon, 2011).

[b]Normal value range: 32–36 g/dl (Turgeon, 2011).

[c]Normal value range: 11.5–14.5% (Turgeon, 2011).

The mean corpuscular volume, the mean corpuscular hemoglobin concentration, and the red blood cell distribution width were determined using an automated blood cell counter certified and used for clinical applications. Volume, surface area, and reduced volume were determined using the quantitative imaging and 3D reconstruction approach described herein. A comparative assessment of the two methods is performed in supplementary Figure S1. Where indicated, the mean ± SD of (*n*) determinations is provided.

Hb, hemoglobin; MCHC, mean corpuscular hemoglobin concentration; MCV, mean corpuscular volume; RDW, red blood cell distribution width.

moment in the parasite's life cycle when the mature merozoites are ready to be released from the infected cell.

We next superimposed the predictions made by the colloid-osmotic model on volume expansion on our experimental data and found a striking agreement (Figure 4a). Note that the numeric model was not fitted to our data, but rather the simulated temporal changes in infected erythrocyte and parasite volume were projected over the empirical data. Also note that none of the parameters considered in the simulation were altered from their original setting. To assess how well the model describes the data, we calculated the difference between the empirical and predicted values and plotted the resulting residuals as a function of the time course of parasite development (Figure 4c). Overall, the residuals were randomly distributed across the x-axis as confirmed by calculating the mean of the residuals, which did not significantly differ from zero (.02 ± .03). This finding, together with the calculated R^2 value of .85, indicates that the colloid-osmotic model can account for the experimental data with high confidence. Furthermore, there was a good agreement between the empirical and predicted parasite volumes (Figure 4a). However, the limited number of data points precluded a thorough statistical analysis.

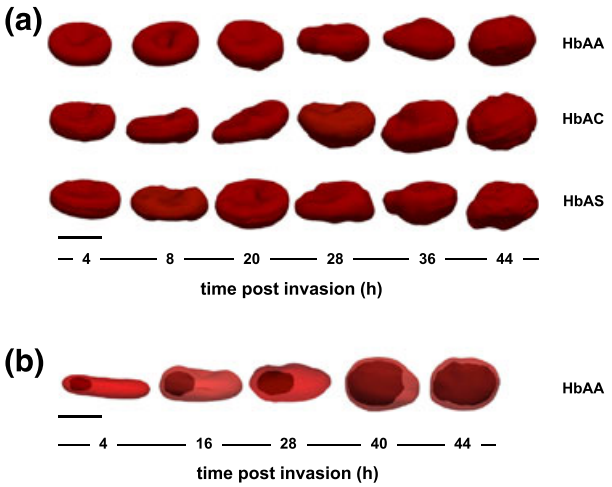

FIGURE 2 Surface rendered views of parasitized erythrocytes. (a) Surface rendered views of parasitized HbAA, HbAC, and HbAS erythrocytes at different stages of parasite development. (b) Surface rendered views of parasitized HbAA erythrocytes including the intracellular pathogen. Scale bars, 5 µm

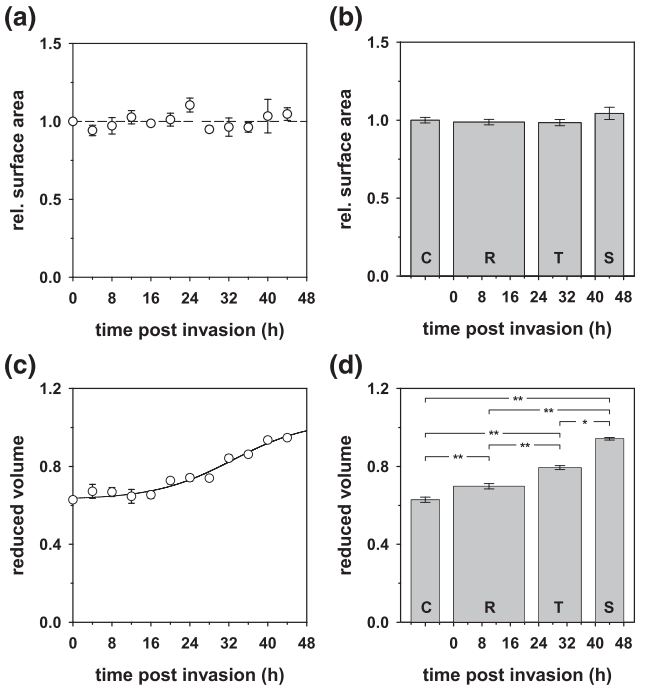

FIGURE 3 Temporal changes in surface area and reduced volume of parasitized HbAA erythrocytes during intraerythrocytic development. (a) Surface area values were normalized to the corresponding means in the uninfected erythrocyte cohort. (b) The same data are shown in a, but values were grouped into uninfected erythrocytes (referred to as controls, C) and ring (R, 0 to 20 hr post invasion), trophozoite (T, 24 to 36 hr post invasion), and schizont stages (S, 40 to 48 hr post invasion). (c) Reduced volume as a function of time post invasion. A four-parameter sigmoidal function was fitted to the data points (R^2 = .998). (d) The same data as in c, but grouped according to parasite stage. Statistical significance was determined using the Kruskal–Wallis one-way analysis of variance on ranks test (*p < .05, **p < .001). The means ± SEM are shown of at least 30 determinations from three independent biological replicates, as defined by using blood from different donors

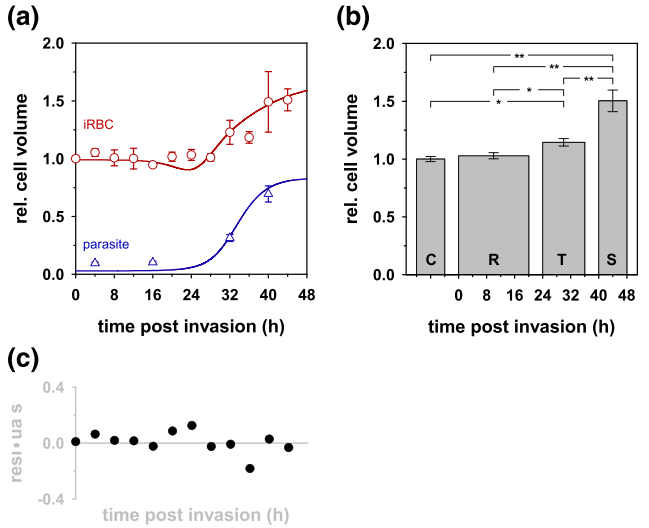

FIGURE 4 Time-dependent changes in cell volume of parasitized HbAA erythrocytes during intraerythrocytic development. (a) Experimentally determined volume of infected erythrocytes (infected red blood cell, iRBC) were normalized to the corresponding mean in the uninfected erythrocyte cohort (open red circles). Blue triangles indicate experimentally determined volumes of the intracellular parasite. Solid lines show the time-dependent volume expansion of the infected erythrocyte (red line) and the parasite (blue line) as predicted by the colloid-osmotic model. The default parameters were used for the simulation. (b) The same data are shown in a, but values were grouped according to parasite stage. (c) Residual plot. The difference between the experimentally derived data and the predicted values was calculated, and the resulting residuals were displayed as a function of the time post invasion. The residuals were analyzed and plotted according to Cornish-Bowden (2001) (Cornish-Bowden, 2001). Statistical significance was determined using the Kruskal–Wallis One Way ANOVA on Ranks test (*p < .05, **p < .001). The means ± SEM of at least 30 determinations, from three independent biological replicates as defined by using blood from different donors, are shown. C, uninfected erythrocytes; R, rings; T, trophozoites; S, schizonts

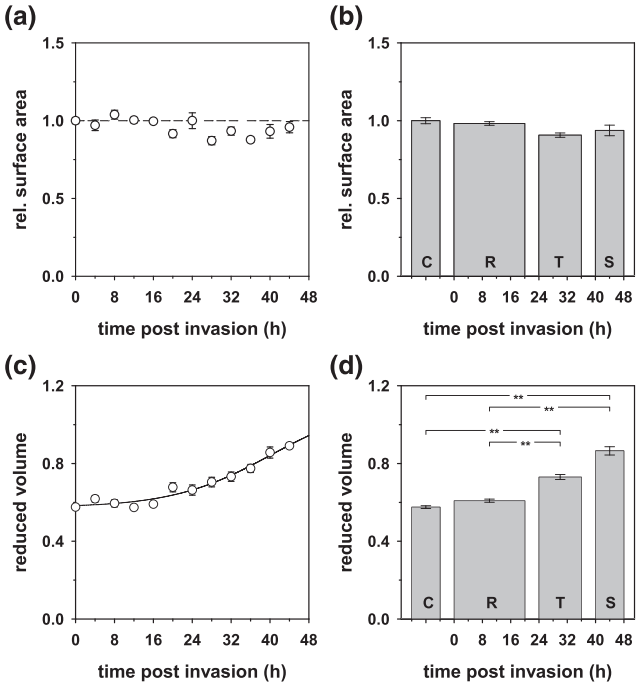

FIGURE 5 Time-dependent changes in surface area and reduced volume of parasitized HbAC erythrocytes during intraerythrocytic development. (a) Normalized surface area of infected erythrocytes. (b) The same data as in a, but grouped according to parasite stage. (c) Reduced volume. A four-parameter sigmoidal function was fitted to the data points (R^2 = .98). (d) Same data as in c, but grouped according to parasite stage. Statistical significance was determined using the Kruskal–Wallis one-way analysis of variance on ranks test (*p < .05, **p < .001). The means ± SEM are shown of at least 30 determinations from three independent biological replicates as defined by using blood from different donors. C, uninfected erythrocytes; R, rings; T, trophozoites; S, schizonts

Contrasting with the overall good agreement between model predictions and empirical data, there seems to be one noticeable discrepancy. The simulation predicts a K^+ driven shrinkage of infected cell volume approximately 24 hr post invasion (Mauritz et al., 2009), which is not obvious in our data set. We refer to the discussion for possible explanations.

2.2 | Delayed NPP activation in parasitized HbAC and HbAS erythrocytes

We repeated the study, but this time, we investigated parasitized HbAC and HbAS erythrocytes. Again, samples were taken from highly synchronized cultures at 4-hr intervals throughout the 48-hr intraerythrocytic developmental cycle and processed for cell surface and volume determinations. As already seen for parasitized HbAA erythrocytes, the surface area of parasitized HbAC erythrocytes remained constant, whereas the reduced and absolute volumes increased with time post invasion (Figures 5 and 6). A linear regression analysis of the cell surface areas determined over the time course of the intraerythrocytic cycle gave a slope not significantly different from zero (Figure 5a). Furthermore, grouping the data according to the developmental stage of the parasite revealed no statistically supported evidence of surface area loss (Figures 5b). With regard to the reduced volume, this parameter significantly increased in a sigmoidal fashion from .58 to .89 determined at the beginning and at the end of the intraerythrocytic developmental cycle, respectively (p < .01; Figure 5c and d). Apparently, the infected cell became more spherical with time as the parasite matured, with the inflection point occurring approximately 32 ± 3 hr post invasion (Figure 5c). The third feature shared with parasitized HbAA erythrocytes is the significant expansion in infected cell volume (p < .05; Figure 6a and b). At the end of the 48-hr cycle, the volume of the infected HbAC cell had expanded by approximately 40 ± 10% (Figures 6a and b).

In spite of comparable temporal surface and volumetric changes, there are clear distinctions between parasitized HbAC and HbAA erythrocytes with regard to the compatibility of the empirical data with the predictions made by the colloidal osmotic model. It is evident from Figure 6a that the model overestimates both infected erythrocyte and parasite volume expansion (dotted lines in Figure 6a).

A critical parameter driving volume expansion in the model is the time point when the activity of the parasite-induced solute channels has reached 50% of its maximum. This parameter is set at 27 hr post invasion (Mauritz et al., 2009), based on empirical evidence derived from permeability studies using sorbitol, alanine, and other solutes to

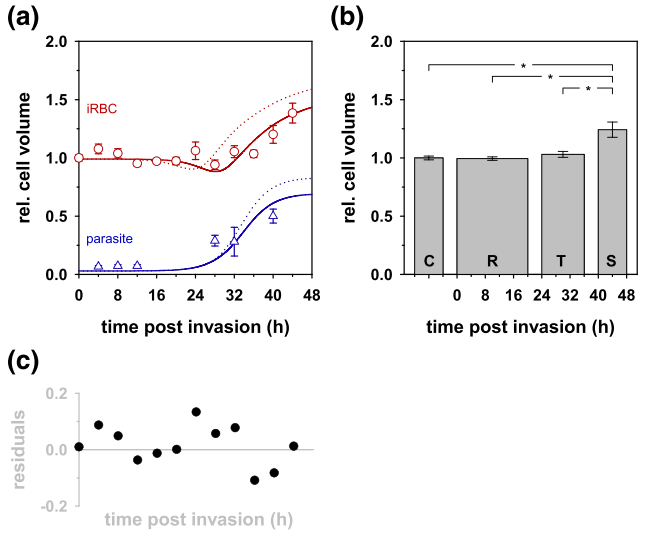

FIGURE 6 Time-dependent changes in cell volume of parasitized HbAC erythrocytes during intraerythrocytic development. (a) Normalized experimentally determined volume of infected erythrocytes (open red circles) and the intracellular parasite (open blue triangles) were superimposed on the predicted values, with the dotted lines indicating a simulation without parameter adjustments, whereas the solid lines indicate a simulation with the half-maximal new permeation pathway induction curve adjusted to 31 hr post invasion. (b) The same data are shown in a, but values were grouped according to parasite stage. (c) Residuals between the experimentally derived and the predicted volumes of infected erythrocytes (values were taken from the adjusted simulation). Statistical significance was determined using the Kruskal–Wallis one-way analysis of variance on ranks test (*$p < .05$, **$p < .001$). The means ± SEM of at least 30 determinations, from three independent biological replicates as defined by using blood from different donors, are shown. C, uninfected erythrocytes; R, rings; T, trophozoites; S, schizonts

probe for the induction of these new permeation pathways in the host cell plasma membrane (Ginsburg et al., 1985; Kirk, 2001; Staines et al., 2001). These experiments, however, were performed with parasitized HbAA erythrocytes and not with parasitized HbAC erythrocytes.

In a previous study, we have shown that export of parasite-encoded proteins to the erythrocyte compartment is delayed and slower in HbAC erythrocyte as compared with HbAA red blood cells (Kilian et al., 2015). Aberrant protein export affects both soluble proteins directed to the host cell cytosol and trans-membrane proteins allotted to the erythrocyte plasma membrane. Extrapolating these findings to the new permeation pathways would suggest that the trafficking of the solute channel proteins to the infected erythrocyte plasma membrane is likewise affected. We reasoned that a slower and delayed export of the NPP channels might shift the half-time of the NPP induction curve to later time points. We explored this possibility by varying this parameter and keeping all other parameters constant in the simulation. A value of 31 hr for the half-time of the NPP induction curve provided the best results. Now the model can explain the empirical data on infected erythrocyte and parasite volume expansion in parasitized HbAC erythrocytes with high confidence (R^2 of .81; solid line in Figure 6a). The good correlation between empirical and simulated data was confirmed by plotting the residuals, which were randomly distributed (Figure 6c), and by calculating the mean of the residuals, which was not significantly different from zero (.01 ± .02).

To validate the predicted delayed activation of the NPPs, we assessed the time-dependent permeability of the host's plasma membrane for sorbitol. The permeability studies were performed in concurrent assays with parasitized HbAA erythrocytes as reference. In the case of parasitized HbAA erythrocytes, we found 50% of the maximal NPP development at time point 26 ± 2 hr post invasion (Figure 7), consistent with previous reports (Staines et al., 2001). In comparison, the NPP induction curve was shifted to later time points in parasitized HbAC and HbAS erythrocytes (Figure 7). In addition, the maximal level of NPP development was lower in the parasitized hemoglobinopathic red blood cells. The differences in the time courses of NPP development were found to be statistically significant between parasitized HbAA and HbAC erythrocytes ($F = 20.0$; DF: 3 and 14; $p > .001$) and between parasitized HbAA and HbAS erythrocytes ($F = 54.1$; DF: 3 and 13; $p > .001$), according to an F-test. No statistical significance was observed between infected HbAS and HbAC erythrocytes ($F = 0.38$; DF: 3, and 13; $p > .77$). Importantly, a degree of NPP development comparable with 50% activation in parasitzed HbAA erythrocytes was reached four hours later at time point 30 ± 2 hr in parasitized HbAC and HbAS erythrocytes (Figure 7). Thus, the experimental and the predicted time-dependent development of the NPPs are in good agreement for parasitized HbAC erythrocyte and can fully account for the differential volume expansion observed in these host cells, compared with parasitized HbAA erythrocytes.

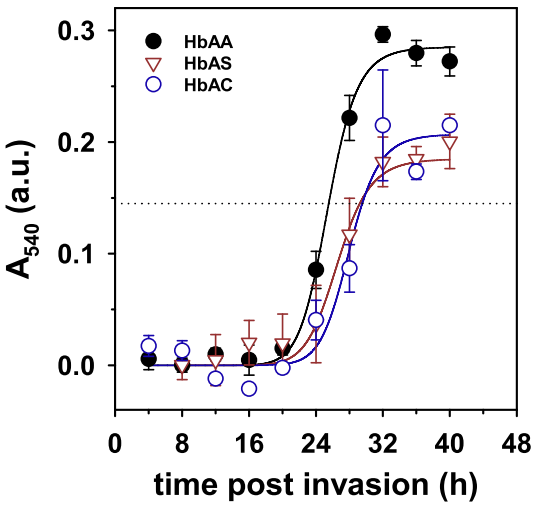

FIGURE 7 New permeation pathway (NPP) induction curves in parasitized HbAA, HbAC, and HbAS erythrocytes. NPP development was assessed by sorbitol-induced hemolysis of parasitized erythrocytes during the replicative cycle. The amount of released hemoglobin was determined by absorption spectroscopy at a wavelength of 540 nm (A_{540}). The means ± SEM of three independent biological replicates, each performed using blood from a different donor, are shown. The dotted line indicates 50% NPP induction in parasitized HbAA erythrocytes. A three-parameter Hill function was fitted to the data points, and statistical significance between the different time courses of NPP activation was evaluated using F statistics (between HbAA and HbAC: $p > .001$; between HbAA and HbAS erythrocytes: $p > .001$; and between HbAS and HbAC: $p > .77$). a.u., arbitrary units

2.3 | Substantial surface area loss in parasitized HbAS erythrocytes

In the case of parasitized HbAS erythrocytes, host cell surface area significantly decreased with time (Figure 8a and b) ($p < .01$). We confirmed the loss in surface area in three independent biological replicates using fresh HbAS erythrocytes from different donors. On average, between 13% and 19% of the infected cell surface area was lost during parasite development. Further setting parasitized HbAS erythrocytes apart was the modest, yet significant increase in reduced volume from .58 to .76 ($p < .01$; Figures 8c and d), indicating a rounding-off of the cell, although not to the same extent as observed in parasitized HbAA and HbAC erythrocytes, consistent with the surface rendered views presented in Figure 2a. Irrespectively, both the surface rendered views and the reduced volumes indicated a swelling of the parasitized HbAS erythrocytes and, hence, an expansion in host cell volume as the parasite matured. Unexpectedly, there was no obvious increase in infected erythrocyte's cell volume (Figure 9a and b). This finding, however, has to be interpreted in light of the surface area loss. The loss in surface area of 13% to 19% would result in a volume reduction of 19% to 27%, assuming a spherical shape and applying the equation $\frac{V1}{V2} = \left(\frac{A1}{A2}\right)^{3/2}$, where V_1 and V_2 and A_1 and A_2 are volume and surface area of two spheres, respectively. Thus, the shrinkage in the volume of the infected erythrocyte due to a loss in surface area and the expansion in volume due to parasite-induced influx of osmotic water appeared to have offset each other in parasitized HbAS erythrocytes, resulting in what appeared to be a constant infected cell volume during parasite development.

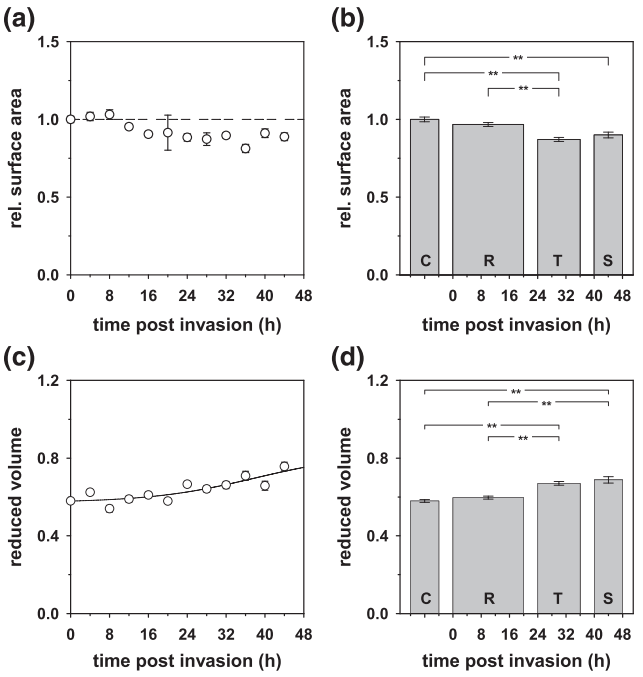

FIGURE 8 Time-dependent changes in surface area and reduced volume of parasitized HbAS erythrocytes during intraerythrocytic development. (a) Normalized surface area of parasitized erythrocytes. (b) The same data as in a, but grouped according to parasite stage. (c) Reduced volume. A four-parameter sigmoidal function was fitted to the data points ($R^2 = .98$). (d) Same data as in c, but grouped according to parasite stage. Statistical significance was determined using the Kruskal–Wallis one-way analysis of variance on ranks test (*$p < .05$, **$p < .001$). The means ± SEM of at least 30 determinations, from three independent biological replicates as defined by using blood from different donors, are shown. C, uninfected erythrocytes; R, rings; T, trophozoites; S, schizonts

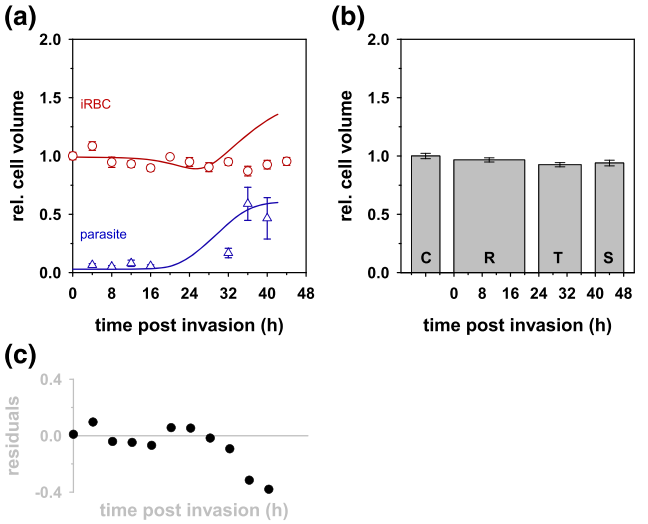

FIGURE 9 Time-dependent changes in cell volume of parasitized HbAC erythrocytes during intraerythrocytic development. (a) Normalized experimentally determined volume of infected erythrocytes (open red circles) and the intracellular parasite (open blue triangles) are shown. The lines indicate the simulated time courses of infected erythrocyte and parasite volume expansion. The following hemoglobin S (HbS)-specific parameters were used in the simulation (solid line): isoelectric pH of HbS, 7.4; mean net charge of HbS, −8.0 equivalents per mol and pH unit; half-maximal new permeation pathway induction curve, 30 hr post invasion; slope of new permeation pathway induction curve, 4. All other parameters were fixed at default values. (b) The same data are shown in a, but data were grouped according to parasite stage. (c) Residuals between the experimentally derived and the predicted infected erythrocyte volumes. Statistical significance was determined using the Kruskal–Wallis one-way analysis of variance on ranks test (*$p < .05$, **$p < .001$). The means ± SEM of at least 30 determinations, from three independent biological replicates as defined by using blood from different donors, are shown. C, uninfected erythrocytes; R, rings; T, trophozoites; S, schizonts

The volumetric simulation by the colloid-osmotic model can consider surface area losses, and it can take into account biochemical parameters specific for HbS, such as the isoelectric pH of 7.4 and the mean net charge of −8.0 equivalents per mol and pH unit. We further considered the altered characteristics of the NPP induction curve compared with parasitized HbAA erythrocytes (Figure 7). However, the results were not satisfactory. The simulation clearly overestimates infected erythrocyte volumes at later time points during the replication cycle (Figure 9a and c). Accordingly, the mean of the residuals was distinct from zero (.10 ± .05) and the R^2 value was low (.45). The simulation, however, accurately predicted the temporal changes in parasite volume, using the settings described earlier (Figure 9a). The resulting curve followed a sigmoidal pattern and was comparable with the volume expansion curves seen for the FCR3 strain grown in HbAA and HbAC erythrocytes (compare the blue curves in Figures 4a, 6a, and 9a). The curves might differ with regard to the slopes and the final plateau values although we could not demonstrate statistical significance.

2.4 | Comparable growth rates and hemozoin production

In previous studies, we have reported comparable multiplication rates of culture-adopted *P. falciparum* strains in HbAA, HbAC, and HbAS erythrocytes (Kilian et al., 2013; Kilian et al., 2015). We confirmed this finding for the *P. falciparum* strain FCR3 used in this study. The FCR3 strain grew with multiplication rates of 10 ± 2 and a cycle length of 48 hr in all three red blood cell variants under continuous in vitro culture conditions, with no statistical difference between the different erythrocyte variants (Table 1). We further quantified the amount of hemozoin present in late trophozoite stages (30 to 36 hr post invasion) as an indicator of Hb digestion. No statistical differences were found between parasitized HbAA, HbAC, and HbAS erythrocytes (Table 1), suggesting comparable rates and amounts of Hb digestion.

3 | DISCUSSION

The colloid-osmotic model predicts time-dependent changes in the volumes of the infected erythrocyte and the intracellular parasite on the basis of ion fluxes across the erythrocyte plasma membrane and on the basis of the rate and amount of Hb consumption. The model further posits that, although the host cell swells as NaCl and accompanying water enter the cell via parasite-induced new permeation pathways, the critical hemolytic volume is approached only at the end of the 48-hr replication cycle. Excessive consumption of osmotically active Hb and the subsequent release of the liberated amino acids into the environment are thought to prevent premature rupture.

The human malaria parasite *P. falciparum* drastically changes the physiological and morphological properties of its host cell during intraerythrocytic development. The parasite creates new permeation pathways, converting the intracellular ion milieu of the host cell into an extracellular environment (Lee, Ye, Van Dyke, & Kirk, 1988; Mauritz et al., 2011; Staines et al., 2001). In addition, the parasite reorganizes the spectrin membrane skeleton of the host erythrocyte. It liberates actin from the junctional complexes (which join spectrin tetramers) to form long actin filaments involved in vesicular trafficking of parasite-encoded proteins to the host cell surface (Cyrklaff et al., 2011; Cyrklaff, Sanchez, Frischknecht, & Lanzer, 2012). The liberated spectrin filaments are used to reinforce parasite-induced protrusions of the erythrocyte plasma membrane, termed knobs (Shi et al., 2013). Knobs play a crucial role in the disease-mediating cytoadhesive behavior of parasitized erythrocytes, by serving as an anchoring platform for the presentation of parasite-encoded adhesins (Crabb et al., 1997).

In the case of parasitized HbAA erythrocytes, there is good agreement between the simulated and the experimentally determined data on volume expansion of the infected erythrocyte and the parasite (Figure 4a). There was no need to evoke a coupling factor linking parasite growth to Hb consumption. The coupling factor was introduced by Mauritz et al. (2009) to reconcile the simulated volumetric data with previous experimental determinations, with the latter falling short of the predicted values (Mauritz et al., 2009). Our results reconcile these earlier studies (Elliott et al., 2001; Elliott et al., 2008; Park et al., 2008; Saliba et al., 1998; Zanner et al., 1990), demonstrating that the colloid-osmotic model quite accurately simulates the volumes of both the infected erythrocyte and the intracellular parasite during the replication cycle (Figure 4a). It is not clear what resulted in the divergent experimental volumetric determinations. However, one might consider sub-optimal culture conditions, strain-dependent variations in intraerythrocytic growth, uncertainties in the measurements, or misjudgment of parasite age. In particular, the later point might be relevant given that parasite and host erythrocyte volume rapidly increase during the second half of intraerythrocytic development. If the age of the parasite is not determined correctly during this phase, it is easy to see how this can interfere with data interpretation.

There was also no need to consider a surface area loss (Esposito et al., 2010). Shedding of membrane by vesiculation is a natural process during red blood cell maturation and senescence, with erythrocytes loosing approximately 16% to 17% of their membrane area during their 120-day life span (Willekens et al., 2008). Vesiculation contributes to the removal of membrane patches damaged by cross-linked non-reducible hemichromes, thereby protecting the red blood cell from premature removal from circulation (Kriebardis et al., 2007; Willekens et al., 2008). Contrasting with previous reports (Esposito et al., 2010; Safeukui et al., 2013; Zanner et al., 1990), we found no evidence of surface area loss in infected HbAA and HbAC erythrocytes during the 48-hr developmental cycle (Figure 3a), provided that red blood cells not older than 2 weeks were used. The exception is parasitized HbAS erythrocytes where the surface area declined with time (Figure 8a). This special case is discussed later. Accelerated vesiculation is a known storage lesion of red blood cells (Kriebardis et al., 2007; van de Watering, 2011), and this might explain why some studies reported shedding of membrane area from infected erythrocytes during the course of parasite maturation (Esposito et al., 2010; Safeukui et al., 2013; Zanner et al., 1990). Unlike other studies, we also did not see echinocytes or stipulated cells, which form under conditions of osmotic stress (Khairy, Foo, & Howard, 2010).

The colloid-osmotic model predicts shrinkage of the infected erythrocyte approximately 24 hr post invasion because of a transient K^+-driven fluid loss brought about by the increased permeability of K^+ over Na^+ and, associated therewith, an asynchronous dissipation of the two electrochemical gradients once the parasite's channels are activated in the erythrocyte plasma membrane (Mauritz et al., 2009). We did not detect this effect, most likely because the volume reduction is very subtle and below the resolution of our approach. Alternatively, the model might overestimate the transient K^+-driven dehydration of the cell.

The colloid-osmotic model can also correctly predict developmental changes in infected erythrocyte and parasite volume in the case of parasitized HbAC erythrocytes (Figure 6a). However, in order to achieve a good correlation between simulated and empirical data, we had to consider the delayed NPP activation (Figure 7). A shift in the NPP induction curve to later time points was experimentally validated and is consistent with comparative protein export studies that have revealed slower and delayed export of parasite-encoded proteins into the host cell compartment of hemoglobinopathic erythrocytes, including HbAC containing red blood cells, compared with HbAA red blood cells (Kilian et al., 2015). It is plausible that impaired export also affects the NPP solute channels, resulting in a delayed Na^+-driven fluid gain

and, hence, a delay in volume expansion. The delayed and reduced activation of the new permeation pathways, as observed in parasitized HbAC and HbAS erythrocytes, might infer a fitness cost to the parasite in the human host (although none was noted under in vitro culture conditions) and, thus, might contribute to the protective function of these structural hemoglobinopathies against severe malaria.

In the case of parasitized HbAS erythrocyte, the infected cell volume exhibited an interesting temporal pattern in that it appeared constant throughout the 48-hr developmental period (Figure 9a). This finding seems to contrast with the surface rendered views and the reduced volumes, which clearly demonstrated a swelling and, hence, an expansion of the infected erythrocyte volume, although not to the extent seen in parasitized HbAA and HbAC erythrocytes (Figures 2a and 8c and d). This apparent contradiction is reconciled by a loss in erythrocyte surface area. Erythrocytes containing HbS have an increased tendency to vesiculate compared with HbAA red blood cells, owing to the instability of HbS and the formation of reactive oxygen species that lead to enhanced amounts of irreversibly oxidized, membrane-associated hemichromes (Chaves, Leonart, & do Nascimento, 2008). Thus, two opposing effects seem to have neutralized each other in the case of parasitized HbAS erythrocytes: the volume expansion due to fluid gain and the volume reduction due to surface area loss. Note that a surface area loss propagates with a volume reduction not in a linear fashion but rather to the power of 1.5, assuming a spherical shape.

In the case of parasitized HbAS erythrocytes, the colloid-osmotic model can explain approximately 45% of the empirical data upon adjustment of the NPP induction curve and taking into account a surface area loss of 16%, an isoelectric pH of 7.4 for HbS, and a mean net charge of −8.0 equivalents per mol and pH unit. However, the simulation overestimates the infected cell volume towards the end of the 48-hr development cycle, while predicting parasite volume expansion with high confidence (Figure 9a and c). It is possible that, at the end of the 48-hr developmental process, the simulation underestimates the numerous effects that HbS has on physiological functions of the red blood cell, which include distorted Ca^{2+}, Na^{+}, and K^{+} homeostasis, redox imbalance, and impaired membrane skeletal organization, among others (Hebbel, 1991).

A recent study has shown that surface area loss and increased sphericity are associated with splenic entrapment of *P. falciparum*-infected erythrocytes (Safeukui et al., 2013). Similarly, senescent red blood cells exhibit reduced surface area, increased sphericity, and decreased deformability, which, in turn, favors their removal from circulation by the spleen (Mohandas & Gallagher, 2008). Given that parasitized HbAS erythrocytes display comparable morphological changes, it is plausible that they are subjected to increased splenic entrapment as compared with parasitized HbAA erythrocytes. Thus, our finding of accelerated vesiculation and, hence, surface area loss while increasing sphericity might lead to a new mechanism by which HbS mitigates disease severity of malaria.

When simulating host erythrocyte and parasite expansion, we assumed that parasite replication rates, replicative cycle length, and Hb consumption were comparable and unaffected by the different Hb variants. Our experimental data support this view. The FCR3 strain grew with comparable replication rate and replicative cycle length in HbAA, HbAC, and HbAS erythrocytes under continuous in vitro culture conditions (Table 1), consistent with previous reports (Kilian et al., 2013; Kilian et al., 2015). We further noted no significant differences in the amount of hemozoin produced in late trophozoites (Table 1), suggesting that Hb degradation progressed at comparable rates and amounts in the different red blood cells investigated.

The colloid-osmotic model predicts that the infected erythrocyte approaches its critical hemolytic volume at the end of the replication cycle. To assess this prediction, we consulted two parameters: the reduced volume and the maximal volume expansion. Changes in both parameters are defined by the biconcave discoid shape of human red blood cells. The biconcave discoid shape is characterized by a high surface to volume ratio, which, in conjunction with the spectrin membrane skeleton, facilitates the repeated, extensive elastic deformations red blood cells encounter while moving through the circulatory system (Diez-Silva, Dao, Han, Lim, & Suresh, 2010; Khairy et al., 2010). As a result of this structural flexibility, red blood cells can expand their volume during osmotic swelling as the erythrocyte becomes spherical, approaching a reduced volume of 1.0 (Ponder, 1948). At 170% of the initial volume, the erythrocyte reaches its critical hemolytic volume and bursts (Ponder, 1948).

It is particularly evident for parasitized HbAA erythrocytes that the volume of the infected erythrocyte reached the maximal possible stable expansion at the end of the replicative cycle, as evidenced by a reduced volume of .99 and a relative volume increase of 60 ± 15% (Figures 3c and 4a). The volume expansions were also critical in parasitized HbAC and HbAS erythrocytes (final reduced volumes of .89 and .76, and relative volume increases of 45–60% and 55 ± 10%; respectively). In the case of parasitized HbAS erythrocytes, a surface area loss of 16% was considered when calculating the maximal volume expansion.

Although infected erythrocytes approach the critical hemolytic volume at the end of the replication cycle, osmotic pressure alone cannot account for the host erythrocyte rupture and merozoite egress. Recent studies have revealed that merozoite egress is a complex programmed event that involves enzymatic modifications of the host cell's plasma membrane and the cytoskeleton by both host and parasite-encoded proteases followed by a spontaneous outward membrane curling and buckling (Abkarian, Massiera, Berry, Roques, & Braun-Breton, 2011; Friedrich, Hagedorn, Soldati-Favre, & Soldati, 2012). Given that the colloid-osmotic hypothesis is a pure kinetic model, it does not consider these effects. It also does not consider the extensive remodeling of the host cell by the parasite during intraerythrocytic development and the effects these modifications have on the mechanical properties of the erythrocyte cell membrane and the underlying cytoskeleton. These modifications are not necessarily homogeneous over the area of the envelope because the parasite positions itself off-center within the red blood cell (Figure 2b). Consistent with this observation, it was found that the reorganization of host cell actin progresses asynchronously within the parasitized erythrocyte, with the distance between the erythrocyte plasma membrane and parasite-induced membrane profiles, termed Maurer's clefts,

reciprocally correlating with the extent of remodeling (Cyrklaff et al., 2011). We therefore envision that a comprehensive description of the rupture process should also include a computer simulation of the spatially resolved mechanics of the infected erythrocyte. The results presented here constitute an ideal starting point to address these important issues.

4 | EXPERIMENTAL PROCEDURES

4.1 | Ethical clearance

The ethical review boards of Heidelberg University and the Biomolecular Research Center (CERBA/Labiogene) approved the study. Written informed consent was obtained from all blood donors after providing oral and written information.

4.2 | Red blood cells

Hemoglobin genotypes were determined by polymerase chain reaction restriction fragment length polymorphism and cellulose acetate electrophoresis as previously described (Modiano et al., 2001). All cells were washed three times with RPMI 1640 medium supplemented with 2-mM L-glutamine, 25-mM Hepes, 100-μM hypoxanthine, 20 μg/ml gentamicin and stored at 4°C until used. All red blood cells were used within 2 weeks after donation.

4.3 | Cell culture

Throughout this study, we used the *P. falciparum* strain FCR3. FCR3 was kept in continuous in vitro culture as described (Trager & Jensen, 2005), using the appropriate red blood cells. Briefly, blood cultures were grown in 10-ml petri dishes at 37°C under controlled atmospheric conditions of 3% CO_2, 5% O_2, and 92% N_2,and at a humidity of 95%. Cells were grown at a hematocrit of 5.0% and at a parasitemia of no higher than 5%. Cultures were tightly synchronized within a time window of 4 hr using 100 μg/ml heparin (Boyle et al., 2010) and 5% Sorbitol (Lambros & Vanderberg, 1979).

4.4 | Confocal imaging and data acquisition

Cells were taken from culture at the appropriate time post invasion, washed, and resuspended in 300-μl RPMI 1640 medium (pH, 7.4; Life Technologies, Carlsbad, CA, USA) at a hemotocrit of 5%. Cells were subsequently labeled with 5-μM BODIPY TR Ceramid (Invitrogen, Carlsbad, CA, USA) for 30 min at 37°C. BODIPY TR Ceramid does not affect membrane integrity or cell shape (Marks, Bittman, & Pagano, 2008). Cells were allowed to settle on a bovine serum albumin-coated glass slide in 37°C warm RPMI 1640 medium. The cells were then examined with an LSM510 confocal laser scanning microscope (Carl Zeiss, Oberkochen, Germany) with a laser power of 20% at a wavelength of 543 nm. Z-stacks consisting of 60 confocal planes were recorded, with a z-spacing of .15 μm and a pixel size in the xy-plane of .0357 μm. The only cells that were immobile during the time period of image acquisition and that were not in contact with neighboring cells were considered for further analysis. For each time point, approximately 30 cells from three different donors were imaged and processed. To obtain accurate and absolute geometric values, the confocal microscope was calibrated using fluorescent spherical beads of 3.1 μM (Sigma-Aldrich, St. Louis, MO, USA), yielding a scaling factor of .95 for the x- and y-axis and of .58 for the z-axis.

4.5 | Image processing

To increase the image quality and resolution and to reduce blur caused by the imaging process, we performed an automated deconvolution, using AutoQuant X3 (Bitplane AG, Zürich, Switzerland) and 35 iterations of the 3D deconvolution algorithm. For each image, a theoretical point spread function was automatically calculated by the software on the basis of the image metadata. The deconvoluted images were uploaded into Imaris (Bitplane AG) for further processing. A median filter was applied to remove outliers in fluorescence intensity. To generate a triangulated surface from the volume data, we used the semi-automated surface extraction workflow of Imairs. A surface smoothing value of .3 μm was used to avoid a too rough surface because of image noise but still to retain the important morphological features of the red blood cell. The threshold for the surface generation was set such that a closed surface was obtained. For obtaining geometric data on the parasite, the images were deconvoluted using Huygens (Scientific Volume Imaging, Hilversum, the Netherlands) and then surface rendered using Imaris. We used the Visualization Toolkit library (Schroeder & Martin, 2005) to compute the surface area, volume, and the reduced volume (R_v) of the segmented triangulated surfaces, as described (Alyassin, Lancaster, Downs, & Fox, 1994).

$$R_v = \frac{\text{Volume of RBC}}{\text{Volume of sphere with surface area of RBC}} = \frac{6\sqrt{\pi}V}{A^{3/2}}$$

The reduced volume of the reconstructed surface is the ratio of its volume to the volume of the sphere having the same surface area as the reconstructed surface. This shape parameter measures how much the reconstructed surface deviates from a sphere. An ideal sphere has a reduced volume of 1.0.

4.6 | Replication rate

The growth phenotypes and replication rates for FCR3 cultured in HbAA, HbAS, and HbAC erythrocytes were assessed by blood Giemsa-stained blood smears over a period of at least 12 cycles. No differences in replication rates or in the lengths of the replicative cycle (48 hr in all cases) were found.

4.7 | Mathematical model of the homeostasis of *P. falciparum*-infected erythrocytes

Version 02/2008 of the software to run the model of infected red blood cell homeostasis was used in this study (Mauritz et al., 2009). The software was installed on a 32-bit personal computer running under Microsoft Windows. If not indicated otherwise, default parameters were used in the simulations.

4.8 | Iso-osmotic hemolysis of infected erythrocytes

Induction of NPPs was assessed as described (Kirk, Horner, Elford, Ellory, & Newbold, 1994). Briefly, highly synchronized infected erythrocytes were monitored for hemolysis capability over the entire intraerythrocytic cycle. Namely, every 4 hr, 1×10^7 infected erythrocytes were suspended, after washing once in phosphate-buffered saline, in 800 µl of iso-osmotic sorbitol lysis solution (280-mM D-sorbitol; 5-mM HEPES; pH 7.4 with NaOH) for 10 min at 37°C. The osmolarity of the solution was 300 mOsm. After centrifugation, 700 µl of supernatant was used to measure absorbance at 540 nm in order to estimate the Hb concentration. Uninfected erythrocytes were assessed in parallel. Each sample was measured in duplicates, and each data point was supported by at least three independent determination using blood from different donors. The stage of parasite development was monitored throughout the experiment using Giemsa-stained blood smears.

4.9 | Quantification of hemozoin levels

The amount of hemozoin was determined as previously described (Schwarzer et al., 1992). Briefly, 2.5×10^8 infected erythrocytes at late trophozoite stages were collected by centrifugation and washed twice with phosphate-buffered saline. The pellet was then osmotically lysed by adding 50 ml of ice-cold distilled water before centrifugation at 4000 rpm at 4°C for 30 min to precipitate the hemozoin and the membrane ghosts. After the centrifugation, the white layer of red blood cell membrane ghosts was aspirated and the hemozoin pellet underneath washed twice with ice-cold distilled water. These were then dissolved in 1 ml of 0.1 M NaOH and incubated at 50°C for 10 min. One hundred microliters of each sample was added to 96-well plates, and the absorbance at 400 nm was determined. The concentration of hemozoin present in each sample was extrapolated from a standard curve of a serial dilution of 0.1 M hemin chloride (Sigma Aldrich).

4.10 | Statistical analysis

Data were analyzed using Sigma Plot 13 (Systat, Chicago, IL, USA). For investigating statistical significance, the Kruskal–Wallis one-way analysis of variance on ranks test or the one-way analysis of variance test was used, as indicated in the figure legends. For method comparison, we used the Bland-Altman test (Bland & Altman, 1986). The NPP induction curves were compared using the *F*-test. Briefly, a three-parameter Hill function was fitted to each data set, and the residual sum of squares (RSS_n) and the degrees of freedom (DF_n) were calculated. Then, the data sets of the two induction curves to be compared were combined, and a three-parameter Hill function was fitted to the combined data set, yielding the residual sum of squares and the degrees of freedom for the fit to the combined data set. The *F* factor was subsequently calculated using the following equation:

$$F = \frac{\frac{(RSS_{1+2} - (RSS_1 + RSS_2))}{(DF_{1+2} - (DF_1 + DF_2))}}{\frac{(RSS_1 + RSS_2)}{(DF_1 + DF_2)}},$$

where RSS_1 and RSS_2 and DF_1 and DF_2 are the residuals sum of squares and the degrees of freedom of the fits to data sets 1 and 2, respectively. RSS_{1+2} and DF_{1+2} refer to the residuals sum of squares and the degrees of freedom of the combined data set 1 and 2. The *F* factor was subsequently converted into a *p* value.

ACKNOWLEDGMENTS

We thank S. Prior and M. Müller for technical assistance and help. We are grateful to J. Kunz and his coworkers at the Zentrum für Kinder- und Jugendmedizin Heidelberg and S. Lobitz at the Klinik für Pädiatrie, Charité Berlin, for providing us with red blood cell variants. We thank Dr. V. Laketa from DZIF for the support with the imaging software Imaris. We are particularly grateful to V. L. Lew for stimulating discussion and for providing the software to run the model of infected red blood cell homeostasis. This work was supported by the Deutsche Forschungsgemeinschaft under the Collaborative Research Center SFB 1129 (project 4). U. S. S. and M. L. are members of the cluster of excellence CellNetworks, and U. S. S. is a member of the Interdisciplinary Center for Scientific Computing (IWR). The authors declare no conflicts of interest.

REFERENCES

Abkarian, M., Massiera, G., Berry, L., Roques, M., & Braun-Breton, C. (2011). A novel mechanism for egress of malarial parasites from red blood cells. *Blood*, *117*, 4118–4124.

Allen, R. J., & Kirk, K. (2004). Cell volume control in the *Plasmodium*-infected erythrocyte. *Trends in Parasitology*, *20*, 7–10. discussion 10-11

Alyassin, A. M., Lancaster, J. L., Downs, J. H. 3rd, & Fox, P. T. (1994). Evaluation of new algorithms for the interactive measurement of surface area and volume. *Medical Physics*, *21*, 741–752.

Bland, J. M., & Altman, D. G. (1986). Statistical methods for assessing agreement between two methods of clinical measurement. *Lancet*, *1*, 307–310.

Boyle, M. J., Wilson, D. W., Richards, J. S., Riglar, D. T., Tetteh, K. K., Conway, D. J., … Beeson, J. G. (2010). Isolation of viable *Plasmodium falciparum* merozoites to define erythrocyte invasion events and advance vaccine and drug development. *Proceedings of the National Academy of Sciences of the United States of America*, *107*, 14378–14383.

Chaves, M. A., Leonart, M. S., & do Nascimento, A. J. (2008). Oxidative process in erythrocytes of individuals with hemoglobin S. *Hematology*, *13*, 187–192.

Cholera, R., Brittain, N. J., Gillrie, M. R., Lopera-Mesa, T. M., Diakite, S. A., Arie, T., … Fairhurst, R. M. (2008). Impaired cytoadherence of *Plasmodium falciparum*-infected erythrocytes containing sickle hemoglobin. *Proceedings of the National Academy of Sciences of the United States of America*, *105*, 991–996.

Cornish-Bowden, A. (2001). Detection of errors of interpretation in experiments in enzyme kinetics. *Methods*, *24*, 181–190.

Crabb, B. S., Cooke, B. M., Reeder, J. C., Waller, R. F., Caruana, S. R., Davern, K. M., … Cowman, A. F. (1997). Targeted gene disruption shows that knobs enable malaria-infected red cells to cytoadhere under physiological shear stress. *Cell*, *89*, 287–296.

Cyrklaff, M., Sanchez, C. P., Frischknecht, F., & Lanzer, M. (2012). Host actin remodeling and protection from malaria by hemoglobinopathies. *Trends in Parasitology*, *28*, 479–485.

Cyrklaff, M., Sanchez, C. P., Kilian, N., Bisseye, C., Simpore, J., Frischknecht, F., & Lanzer, M. (2011). Hemoglobins S and C interfere with actin remodeling in *Plasmodium falciparum*-infected erythrocytes. *Science*, *334*, 1283–1286.

Dalia, S., & Zhang, L. (2013). Homozygous hemoglobin C disease. *Blood*, *122*, 1694.

Desai, S. A. (2012). Ion and nutrient uptake by malaria parasite-infected erythrocytes. *Cellular Microbiology*, *14*, 1003–1009.

Diez-Silva, M., Dao, M., Han, J., Lim, C. T., & Suresh, S. (2010). Shape and biomechanical characteristics of human red blood cells in health and disease. *MRS Bulletin*, *35*, 382–388.

Elliott, D. A., McIntosh, M. T., Hosgood, H. D. 3rd, Chen, S., Zhang, G., Baevova, P., & Joiner, K. A. (2008). Four distinct pathways of hemoglobin uptake in the malaria parasite *Plasmodium falciparum*. *Proceedings of the National Academy of Sciences of the United States of America*, *105*, 2463–2468.

Elliott, J. L., Saliba, K. J., & Kirk, K. (2001). Transport of lactate and pyruvate in the intraerythrocytic malaria parasite, *Plasmodium falciparum*. *Biochemical Journal*, *355*, 733–739.

Esposito, A., Choimet, J. B., Skepper, J. N., Mauritz, J. M., Lew, V. L., Kaminski, C. F., & Tiffert, T. (2010). Quantitative imaging of human red blood cells infected with *Plasmodium falciparum*. *Biophysical Journal*, *99*, 953–960.

Fairhurst, R. M., Baruch, D. I., Brittain, N. J., Ostera, G. R., Wallach, J. S., Hoang, H. L., … Wellems, T. E. (2005). Abnormal display of PfEMP-1 on erythrocytes carrying haemoglobin C may protect against malaria. *Nature*, *435*, 1117–1121.

Fairhurst, R. M., & Casella, J. F. (2004). Images in clinical medicine. Homozygous hemoglobin C disease. *The New England Journal of Medicine*, *350*, e24.

Friedrich, N., Hagedorn, M., Soldati-Favre, D., & Soldati, T. (2012). Prison break: Pathogens' strategies to egress from host cells. *Microbiology and Molecular Biology Reviews*, *76*, 707–720.

Ginsburg, H., Kutner, S., Krugliak, M., & Cabantchik, Z. I. (1985). Characterization of permeation pathways appearing in the host membrane of *Plasmodium falciparum* infected red blood cells. *Molecular and Biochemical Parasitology*, *14*, 313–322.

Ginsburg, H., & Stein, W. D. (2004). The new permeability pathways induced by the malaria parasite in the membrane of the infected erythrocyte: Comparison of results using different experimental techniques. *The Journal of Membrane Biology*, *197*, 113–134.

Hannemann, A., Weiss, E., Rees, D. C., Dalibalta, S., Ellory, J. C., & Gibson, J. S. (2011). The properties of red blood cells from patients heterozygous for HbS and HbC (HbSC genotype). *Anemia*, *2011*, 248527.

Hebbel, R. P. (1991). Beyond hemoglobin polymerization: The red blood cell membrane and sickle disease pathophysiology. *Blood*, *77*, 214–237.

Khairy, K., Foo, J., & Howard, J. (2010). Shapes of Red Blood Cells: Comparison of 3D confocal images with the bilayer-couple model. *Cellular and Molecular Bioengineering*, *1*, 173–181.

Kilian, N., Dittmer, M., Cyrklaff, M., Ouermi, D., Bisseye, C., Simpore, J., … Lanzer, M. (2013). Haemoglobin S and C affect the motion of Maurer's clefts in *Plasmodium falciparum*-infected erythrocytes. *Cellular Microbiology*, *15*, 1111–1126.

Kilian, N., Srismith, S., Dittmer, M., Ouermi, D., Bisseye, C., Simpore, J., … Lanzer, M. (2015). Hemoglobin S and C affect protein export in *Plasmodium falciparum*-infected erythrocytes. *Biology Open*, *4*, 400–410.

Kirk, K. (2001). Membrane transport in the malaria-infected erythrocyte. *Physiological Reviews*, *81*, 495–537.

Kirk, K., Horner, H. A., Elford, B. C., Ellory, J. C., & Newbold, C. I. (1994). Transport of diverse substrates into malaria-infected erythrocytes via a pathway showing functional characteristics of a chloride channel. *The Journal of Biological Chemistry*, *269*, 3339–3347.

Kriebardis, A. G., Antonelou, M. H., Stamoulis, K. E., Economou-Petersen, E., Margaritis, L. H., & Papassideri, I. S. (2007). Progressive oxidation of cytoskeletal proteins and accumulation of denatured hemoglobin in stored red cells. *Journal of Cellular and Molecular Medicine*, *11*, 148–155.

Krugliak, M., Zhang, J., & Ginsburg, H. (2002). Intraerythrocytic *Plasmodium falciparum* utilizes only a fraction of the amino acids derived from the digestion of host cell cytosol for the biosynthesis of its proteins. *Molecular and Biochemical Parasitology*, *119*, 249–256.

Kwiatkowski, D. P. (2005). How malaria has affected the human genome and what human genetics can teach us about malaria. *American Journal of Human Genetics*, *77*, 171–192.

Lambros, C., & Vanderberg, J. P. (1979). Synchronization of *Plasmodium falciparum* erythrocytic stages in culture. *The Journal of Parasitology*, *65*, 418–420.

Lee, P., Ye, Z., Van Dyke, K., & Kirk, R. G. (1988). X-ray microanalysis of *Plasmodium falciparum* and infected red blood cells: Effects of qinghaosu and chloroquine on potassium, sodium, and phosphorus composition. *The American Journal of Tropical Medicine and Hygiene*, *39*, 157–165.

Lew, V. L., & Bookchin, R. M. (2005). Ion transport pathology in the mechanism of sickle cell dehydration. *Physiological Reviews*, *85*, 179–200.

Lew, V. L., Macdonald, L., Ginsburg, H., Krugliak, M., & Tiffert, T. (2004). Excess haemoglobin digestion by malaria parasites: A strategy to prevent premature host cell lysis. *Blood Cells, Molecules & Diseases*, *32*, 353–359.

Lew, V. L., Tiffert, T., & Ginsburg, H. (2003). Excess hemoglobin digestion and the osmotic stability of *Plasmodium falciparum*-infected red blood cells. *Blood*, *101*, 4189–4194.

Lim, H. W. G., Wortis, M., & Mukhopadhyay, R. (2002). Stomatocyte-discocyte-echinocyte sequence of the human red blood cell: evidence for the bilayer- couple hypothesis from membrane mechanics. *Proceedings of the National Academy of Sciences of the United States of America*, *99*, 16766–16769.

Lim, H. W. G., Wortis, M., & Mukhopadhyay, R. (2008). Red blood cell shapes and shape transformations: newtonian mechanics of a composite membrane. In G. Gompper, & M. Schick (Eds.), *Soft matter* (pp. 83–139). Weinheim: WILEY-VCH Verlag GmbH & Co. KGaA.

Marks, D. L., Bittman, R., & Pagano, R. E. (2008). Use of Bodipy-labeled sphingolipid and cholesterol analogs to examine membrane microdomains in cells. *Histochemistry and Cell Biology*, *130*, 819–832.

Mauritz, J. M., Esposito, A., Ginsburg, H., Kaminski, C. F., Tiffert, T., & Lew, V. L. (2009). The homeostasis of *Plasmodium falciparum*-infected red blood cells. *PLoS Computational Biology*, *5*, e1000339.

Mauritz, J. M., Seear, R., Esposito, A., Kaminski, C. F., Skepper, J. N., Warley, A., … Tiffert, T. (2011). X-ray microanalysis investigation of the changes in Na, K, and hemoglobin concentration in *Plasmodium falciparum*-infected red blood cells. *Biophysical Journal*, *100*, 1438–1445.

Modiano, D., Luoni, G., Sirima, B. S., Simpore, J., Verra, F., Konate, A., … Coluzzi, M. (2001). Haemoglobin C protects against clinical *Plasmodium falciparum* malaria. *Nature*, *414*, 305–308.

Mohandas, N., & Gallagher, P. G. (2008). Red cell membrane: Past, present, and future. *Blood*, *112*, 3939–3948.

Nagel, R. L., Fabry, M. E., & Steinberg, M. H. (2003). The paradox of hemoglobin SC disease. *Blood Reviews*, *17*, 167–178.

Nash, G. B., O'Brien, E., Gordon-Smith, E. C., & Dormandy, J. A. (1989). Abnormalities in the mechanical properties of red blood cells caused by *Plasmodium falciparum*. *Blood*, *74*, 855–861.

Park, Y., Diez-Silva, M., Popescu, G., Lykotrafitis, G., Choi, W., Feld, M. S., & Suresh, S. (2008). Refractive index maps and membrane dynamics of human red blood cells parasitized by *Plasmodium falciparum*. *Proceedings of the National Academy of Sciences of the United States of America*, *105*, 13730–13735.

Ponder, E. (1948). *Hemolysis and related phenomenon*New York: Grune & Stratton.

Rosenthal, P. J. (2011). Falcipains and other cysteine proteases of malaria parasites. *Advances in Experimental Medicine and Biology*, *712*, 30–48.

Safeukui, I., Buffet, P. A., Perrot, S., Sauvanet, A., Aussilhou, B., Dokmak, S., … Milon, G. (2013). Surface area loss and increased sphericity account for the splenic entrapment of subpopulations of *Plasmodium falciparum* ring-infected erythrocytes. *PloS One*, *8*, e60150.

Saliba, K. J., Horner, H. A., & Kirk, K. (1998). Transport and metabolism of the essential vitamin pantothenic acid in human erythrocytes infected with the malaria parasite *Plasmodium falci'parum*. *The Journal of Biological Chemistry*, *273*, 10190–10195.

Schroeder, W.J., & Martin, K.M. (2005). The visualization toolkit. *Vis Handb*, 593–614.

Schwarzer, E., Turrini, F., Ulliers, D., Giribaldi, G., Ginsburg, H., & Arese, P. (1992). Impairment of macrophage functions after ingestion of *Plasmodium falciparum*-infected erythrocytes or isolated malarial pigment. *The Journal of Experimental Medicine*, *176*, 1033–1041.

Shi, H., Liu, Z., Li, A., Yin, J., Chong, A. G., Tan, K. S., … Lim, C. T. (2013). Life cycle-dependent cytoskeletal modifications in *Plasmodium falciparum* infected erythrocytes. *PloS One*, *8*, e61170.

Staines, H. M., Ellory, J. C., & Kirk, K. (2001). Perturbation of the pump-leak balance for Na(+) and K(+) in malaria-infected erythrocytes. *American Journal of Physiology. Cell Physiology*, *280*, C1576–C1587.

Taylor, S. M., Parobek, C. M., & Fairhurst, R. M. (2012). Haemoglobinopathies and the clinical epidemiology of malaria: a systematic review and meta-analysis. *The Lancet Infectious Diseases*, *12*, 457–468.

Trager, W., & Jensen, J. B. (2005). Human malaria parasites in continuous culture. 1976. *The Journal of Parasitology*, *91*, 484–486.

Turgeon, M. L. (2011). *Clinical Hematology: Theory and Procedures 5th edition*, Philadelphia: Lippincott Williams & Wilkins.

van de Watering, L. (2011). Red cell storage and prognosis. *Vox Sanguinis*, *100*, 36–45.

Willekens, F. L., Werre, J. M., Groenen-Dopp, Y. A., Roerdinkholder-Stoelwinder, B., de Pauw, B., & Bosman, G. J. (2008). Erythrocyte vesiculation: A self-protective mechanism? *British Journal of Haematology*, *141*, 549–556.

World Health Organization (2015). *World Malaria Report 2014*, Geneva: WHO Press.

Zanner, M. A., Galey, W. R., Scaletti, J. V., Brahm, J., & Vander Jagt, D. L. (1990). Water and urea transport in human erythrocytes infected with the malaria parasite *Plasmodium falciparum*. *Molecular and Biochemical Parasitology*, *40*, 269–278.

SUPPORTING INFORMATION

Additional Supporting Information may be found online in the supporting information tab for this article.

How to cite this article: Waldecker, M., Dasanna, A. K., Lansche, C., Linke, M., Srismith, S., Cyrklaff, M., Sanchez, C. P., Schwarz, U. S., and Lanzer, M. (2016), Differential time-dependent volumetric and surface area changes and delayed induction of new permeation pathways in *P. falciparum*-infected hemoglobinopathic erythrocytes, *Cellular Microbiology*, doi: 10.1111/cmi.12650